Hybrid Modular Multilevel Converter With Redistributed Power to Reduce Submodule Capacitor Voltage Fluctuation

Ming Huang, Jianlong Zou, and Xikui Ma

***Abstract*—This paper introduces a hybrid modular multilevel converter (MMC) with the full-bridge submodules (FBSMs) inserted in the ac side. It is intended for redistributing arm powers of the MMC system to reduce the submodule (SM) capacitor voltage fluctuation by injecting high-frequency powers in upper and lower arms without disturbing the output voltage. New power distribution of the hybrid MMC system can be realized by controlling the SMs and FBSMs working under the high-frequency powers. The proposed FBSMs in the hybrid MMC system also perform as the harmonic power generator to eliminate the common-mode voltages in the ac side. Since the FBSMs locate in the ac side of the hybrid MMC system, the traditional MMC control method can be directly applied in arm control of the hybrid MMC system. Meanwhile, relationship between the arm powers and SM capacitor voltage has been analyzed in detail to reduce the SM capacitor voltage ripples by redistributing the frequency spectrum of arm powers. Simulation and experimental results have also verified the effectiveness of the proposed method.**

***Index Terms*—Capacitor voltage ripples, full-bridge submodule (FBSM), hybrid modular multilevel converter (MMC), power redistribution.**

I. Introduction

RECENTLY, modular multilevel converter (MMC) [1]–[5] has shown great interest in medium- to high-voltage applications due to the merits of modular nature, small step voltage, low loss of switching devices and outstanding ability of fault-clearing. Different from the traditional two-level voltage source converter and the neutral-point-clamped converter [6], MMC has the excellent output voltage and can be easily driven for its modular nature without considering the dynamic performance of single insulated gate bipolar transistor (IGBT). Moreover, the voltage level of MMC can be increased by simply cascading more submodules (SMs). The more the SMs of the MMC system are cascading, the more voltage level of the output waveform can be obtained. Therefore, the *LCL* filter of the traditional two-level voltage source converter (VSC) is no longer necessary for the MMC system with numerous SMs. This makes MMC advantageous in the family of multilevel converters.

Efforts about MMC on circulating current suppression, balancing control, multilevel modulation, topologies, etc., have been done to improve the MMC performance [7]–[11]. However, due to the feature of the traditional MMC topology, imbalance of the upper power and lower power is still the major problem resulting in serious fluctuation in SM capacitor voltage, especially for the low-frequency output operations [12]–[16]. Although the common part of the upper and lower powers can be eliminated by controlling the total energy stored in phases properly for the traditional MMC system, different parts of the upper and lower power still contribute the major of capacitor voltage fluctuation. Several works of literature have been presented to solve this problem [15]–[18]. Literature [15] proposed to inject high-frequency current and voltage in arms to eliminate different parts of upper and lower powers in fundamental frequency, which could dramatically reduce the capacitor voltage fluctuation. However, the injected high-frequency voltages of arms resulting in common-mode voltage in the ac side would damage ac motors in long-time running. Moreover, the zero-crossing point of the injected current reference has to be compromised in sacrifice of precision. Although the square-wave reference method in [16] could get rid of the zero-crossing issue, square-wave currents in arm reactors would result in huge peak voltages. A new MMC with the injected sinusoidal-wave method has been presented in [17] to suppress the capacitor voltage ripples, which does not aim to eliminate the low-frequency different powers in upper and lower arms but to transfer the low-frequency part to the high-frequency part by multiplying a high-frequency sinusoidal wave without suffering the zero-crossing issue. And the switching frequency has not to be high enough. However, new complicated voltage balancing control is performed due to the inserted middle-cell in arms in [17], and the common-mode voltage in the ac side still exists. An effective method for removing the undesired common-mode voltage is presented in [18] by introducing a connected flying capacitor between the upper and lower arms for compensating the imbalanced powers. However, decrease of capacitor

Manuscript received June 20, 2017; revised August 8, 2017; accepted September 15, 2017. Date of publication September 21, 2017; date of current version April 20, 2018. This work was supported in part by the National Natural Science Foundation of China under Grant 51177118 and in part by the Research Fund for the Doctoral Program of Higher Education of China under Grant 20130201110008. Recommended for publication by Associate Editor Navid Reza Zargari. *(Corresponding author: Jianlong Zou.)*

The authors are with the State Key Laboratory of Electrical Insulation and Power Equipment, School of Electrical Engineering, Xi'an Jiaotong University, Xi'an 710049, China (e-mail: huangming@stu.xjtu.edu.cn; superzou@mail.xjtu.edu.cn; maxikui@mail.xjtu.edu.cn).

Color versions of one or more of the figures in this paper are available online at http://ieeexplore.ieee.org.

Digital Object Identifier 10.1109/TPEL.2017.2755763

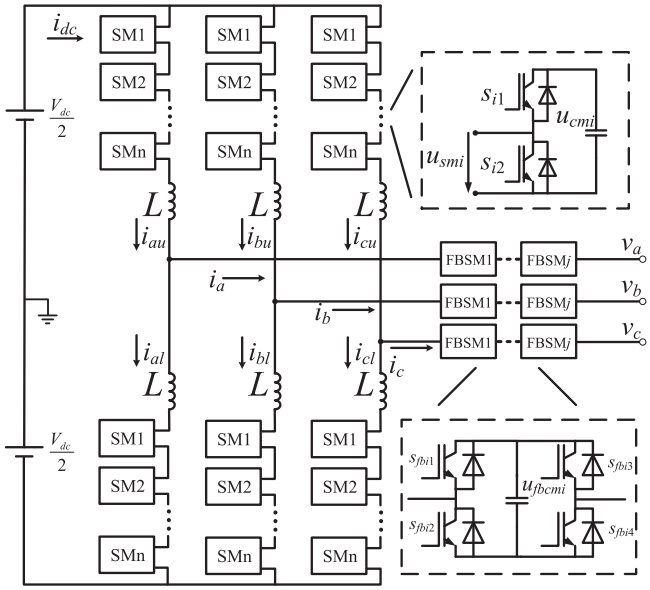

Fig. 1. Configuration of the proposed hybrid MMC topology.

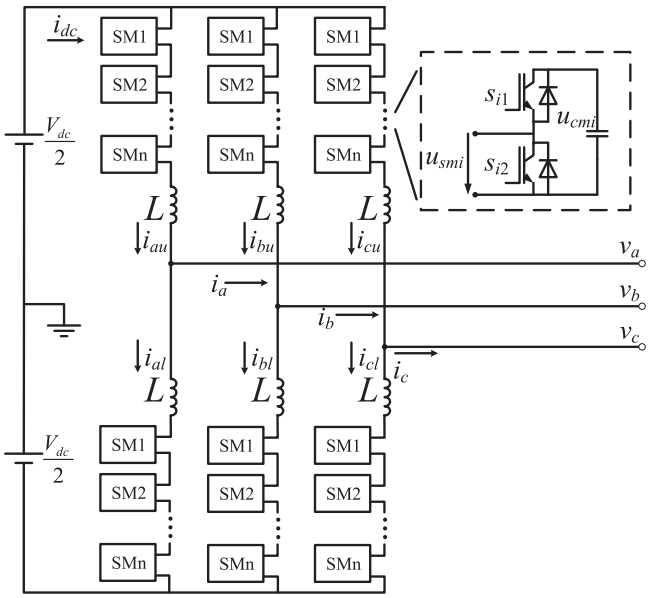

Fig. 2. Configuration of the traditional half-bridge SM-based MMC.

value resulting from the reducing electrolyte in the electrolytic flying capacitor, which mismatches with the resonant frequency in [18], could weaken the compensated system performance in long-term running. Meanwhile, it should be noted that the flying capacitor suffering from the high voltage up to half of the dc bus voltage has to be bulky and costly. A hybrid MMC topology with cascaded full-bridge SMs (FBSMs) in the ac side is presented in [19] mainly to shape the output voltage and cut off the dc fault current. However, the unsmoothed referenced voltage for the FBSMs is not easy to be achieved with a relative low switching frequency. Moreover, the SM capacitor voltages still suffer from the large ripples due to the dominant low-frequency powers among them.

This paper introduces the hybrid MMC topology presented in [19] with cascaded FBSMs inserted in the ac side as shown in Fig. 1, to reduce the SM capacitor voltage fluctuation by redistributing powers in arms without disturbing the output voltage. The FBSMs in the MMC system function as the harmonic power generator to eliminate the undesired harmonic power in the ac side. Different from the modified MMC topology in [17], this topology is free of the complicated voltage balancing control caused by the middle cell in [17]. This means the traditional balancing control and average control in [20] can be directly applied to the proposed MMC system. Moreover, the FBSMs in the ac side of the hybrid MMC could enlarge the modulation index of the proposed MMC system.

This paper is organized as follows. Section II describes the power distribution of the traditional MMC topology and reveals the relationship between SM powers and harmonics of SM capacitor voltage for the cascaded multilevel converter. The hybrid MMC with inserted high-frequency powers in arms is proposed and analyzed in Section III. Simulation and experimental results have verified the effectiveness of the proposed method under the low-frequency output operation in Sections IV and V, respectively. Section VI presents the conclusion of this paper.

II. Traditional MMC Topology Analysis

A. Modeling and Analysis of SM

The basic structure of the traditional half-bridge SM-based MMC is shown in Fig. 2. The converter consists of three phases which can be divided into six arms. Each arm has n half-bridge-based SMs which consist of two IGBTs and an electrolytic capacitor individually. The SMs of each arm operate with complementary switching pulses applied in the two IGBTs under normal condition. The SM capacitors are then chopped by the switches for producing desirable output voltage of the SMs.

With attention focusing on the individual SM, power exchanging between output side and capacitor side of each SM should be balanced due to nonstored energy feature of IGBTs under the normal operation with assumption that the switching losses are ignored. Set the positive current direction as shown in Fig. 2, then the power stored in each SM can be expressed as

$$p_{\mathrm{sm}i} = u_{\mathrm{sm}i} \cdot i_{xy} = u_{\mathrm{cm}i} \cdot C\frac{du_{\mathrm{cm}i}}{dt}, \qquad i = 1, 2, \ldots, n \quad (1)$$

where $p_{\mathrm{sm}i}$, u_{sm}, and $u_{\mathrm{cm}i}$ are the power, output voltage, and capacitor voltage of the ith SM, respectively, i_{xy} is the arm current ($y = u, l$) of phase x ($x = a, b, c$), and C is the capacitor value of individual SM.

For simplification of the analysis, the upper arm of phase a is taken for an example. From (1), the upper arm power of phase a is

$$p_{\mathrm{up}} = \left(\sum_{i=1}^{n} u_{\mathrm{sm}i}\right) \cdot i_{\mathrm{au}} = C\sum_{i=1}^{n}\left(u_{\mathrm{cm}i}\frac{du_{\mathrm{cm}i}}{dt}\right) \quad (2)$$

where p_{up} is the upper arm power.

For analysis of the relationship between arm power and capacitor voltage fluctuation, the SM capacitor voltage can be expressed by the ripple model as

$$u_{\mathrm{cm}i} = u_{\mathrm{cm}} + \Delta u_{\mathrm{cm}i} \quad (3)$$

where $u_{\rm cm}$ is the SM capacitor reference voltage of each SM, and $\triangle u_{{\rm cm}i}$ is the fluctuation of the *i*th SM.

With the reasonable consideration that the SM capacitor voltages have the same behavior in each arm by proper control presented in [20], according to (2) and (3), we obtain

$$p_{\rm up} = \left(\sum_{i=1}^{n} u_{{\rm sm}i}\right) \cdot i_{\rm au} \approx CV_{\rm dc}\frac{d\Delta u_{\rm cmu}}{dt} \tag{4}$$

where $V_{\rm dc}$ is the dc-bus voltage, and $\triangle u_{\rm cmu}$ is the SM capacitor voltage fluctuation of each SM in the upper arm. It should be noted that (4) is under the assumption that the fluctuation of SM capacitor voltage is negligible compared with the SM capacitor reference voltage. It can be seen from (4) that any frequency component in upper arm power also exists in capacitor voltage with proportion. In other words, power distribution in the upper arm is crucial to the frequency spectrum of SM capacitor voltage. Equation (4) reveals the basic relationship between arm power and capacitor voltage under the condition of unchanging the cascaded topology feature of each arm with the unique control method in [20].

B. Analysis of Power Distribution in Arms

For the traditional MMC system, the power distribution in the upper and lower arms cannot be determined just by specifying the dc-bus voltage, the output reference voltage, and load current reference in the ac side. The control structure also contributes influence to the power distribution in arms by inserting different harmonics in circulating current. For the further exploration, references in the ac side of phase *a* can be expressed as

$$\begin{cases} v_a = V_a \sin\omega t \\ i_a = I_a \sin\left(\omega t - \varphi\right) \end{cases} \tag{5}$$

where V_a and I_a are the amplitudes of output voltage v_a and load current i_a, respectively, ω is the angular frequency of the output voltage, and φ is the phase angle. Then, the circulating current can be expressed as

$$i_{da} = i_d + i_{ha} \tag{6}$$

where i_{da} is the circulating current of phase *a*, and i_d and i_{ha} are dc part and high-frequency part, respectively. With symmetrical parameters applied in the three-phase MMC, the dc part of i_{da} contributes one-third of the dc bus current $i_{\rm dc}$. Moreover, with balanced power between the dc side and ac side, the following equation can be achieved:

$$V_{\rm dc} \cdot i_d = \frac{1}{2} V_a \cdot I_a \cos\varphi. \tag{7}$$

Moreover, amplitude of phase *a* can be expressed with the dc-bus voltage and the modulation index *m* as

$$V_a = \frac{1}{2} m V_{\rm dc}. \tag{8}$$

With detailed discussion in [21], the upper and the lower arm powers can be expressed as

$$\begin{cases} p_{\rm up} = \frac{1}{2}V_{\rm dc}\left(i_d + i_{ha}\right) - \frac{1}{2}v_a i_a + \frac{1}{4}V_{\rm dc} i_a - v_a\left(i_d + i_{ha}\right) \\ p_{\rm low} = \frac{1}{2}V_{\rm dc}\left(i_d + i_{ha}\right) - \frac{1}{2}v_a i_a - \frac{1}{4}V_{\rm dc} i_a + v_a\left(i_d + i_{ha}\right) \end{cases}. \tag{9}$$

By substituting (5)–(8) into (9), the following equation can be obtained:

$$\begin{cases} p_{\rm up} = p_{\rm com} + p_{\rm dif} \\ p_{\rm low} = p_{\rm com} - p_{\rm dif} \end{cases} \tag{10}$$

where

$$p_{\rm com} = \frac{1}{2}V_{\rm dc} i_{ha} + \frac{m}{8}V_{\rm dc} I_a \cos\left(2\omega t - \varphi\right) \tag{11}$$

$$p_{\rm dif} = \frac{2-m^2}{8}\cos\varphi V_{\rm dc} I_a \sin\omega t - \frac{2\sin\varphi}{4}V_{\rm dc} I_a \cos\omega t - \frac{m}{2}V_{\rm dc} i_{ha} \sin\omega t \tag{12}$$

where $p_{\rm com}$ is the common-mode part in upper and lower arm powers while $p_{\rm dif}$ is the differential-mode part in upper and lower arm powers.

It can be seen from (10) that the arm powers consist of the common-mode power and the differential-mode power. The common-mode power not only has influence on power distribution in arm branches but also has influence on power distribution in the dc side and ac side. However, unlike the common-mode part, the differential-mode power only flows within the arm branches for power exchanging without disturbing the dc side and ac side. For the traditional three-phase MMC system, it is feasible for us to eliminate the common-mode power in arm branches without injecting harmonics into dc and ac sides. However, the elimination of the common-mode power in arms is at the cost of the injected second-order harmonic in the circulating current for the traditional MMC topology.

C. Frequency Spectral Distribution in Capacitor Voltage

It is important to maintain the SM capacitor voltage in its reference for forming the required output voltage. However, with the unavoidable SM capacitor voltage ripples caused by the power exchange between the ac side and dc side, it is necessary to suppress the capacitor voltage ripples to the acceptable range. Moreover, since the size of the electrolytic capacitor occupies more than half of the volume of single SM, it is significant to reduce the ripples of SM capacitor voltage in order to decrease the size of the bulky capacitor. Therefore, analysis of frequency spectrum distribution in SM capacitor voltage shows an essential position. With (4) and (10), it is assumed that the harmonics of capacitor voltage ripple are expressed in the following form:

$$CV_{\rm dc}\frac{d\Delta u_{\rm cm}}{dt} = p_{\rm com} + p_{\rm dif} = CV_{\rm dc}\sum_{i=1}^{\infty}\frac{df_i(t)}{dt} \tag{13}$$

where $f_i(t)$ is the function of the *i*th harmonic. It is obvious that the SM capacitor voltages and the arm powers include the same frequencies.

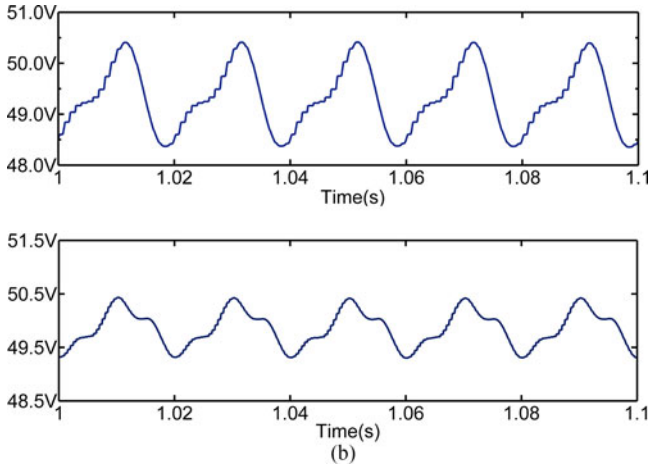

Fig. 3. SM capacitor voltages with $m = 1, \varphi = 0, \omega = 314$ rad/s. (a) Capacitor voltage with injected second harmonic. (b) Capacitor voltage with eliminated second harmonic.

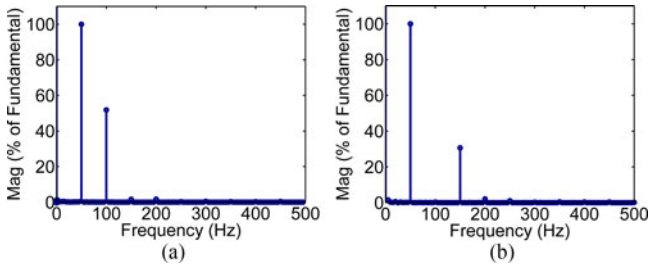

Fig. 4. Frequency distribution of submodule capacitor voltage with $m = 1$, $\varphi = 0, \omega = 314$ rad/s. (a) Frequency distribution of SM capacitor voltage with injected second harmonic. (b) Frequency distribution of SM capacitor voltage with eliminated second harmonic.

With above-mentioned discussion, harmonics of SM capacitor voltage with different control strategies include two situations. Fig. 3 shows the SM capacitor voltages of the two situations. The frequency spectra of Fig. 3 are shown in Fig. 4.

1) Capacitor Voltage With Second Harmonic Injected: The SM capacitor voltage with injected second harmonic means the injected second harmonic in arm powers. In other words, the second harmonic power resulted from load power for the single-phase MMC system can be restored in arms without disturbing the circulating current, which means the circulating current only contains the dc component. Therefore, with (11)–(13), the relationship of arm power and capacitor voltage ripple can be expressed as

$$\sum_{i=1}^{\infty}\frac{df_i(t)}{dt} = \frac{m}{8C}I_a\cos\left(2\omega t-\varphi\right)+\frac{2-m^2}{8C}\cos\varphi I_a\sin\omega t - \frac{2\sin\varphi}{4C}I_a\cos\omega t. \tag{14}$$

It can be seen from (14) that SM capacitor voltage ripples only contain the fundamental frequency and the second harmonic frequency. Therefore, the harmonic components in SM capacitor voltage ripples can be calculated as

$$f_1(t) = -\frac{2-m^2}{8\omega C}\cos\varphi I_a\cos\omega t - \frac{2\sin\varphi}{4\omega C}I_a\sin\omega t \tag{15}$$

$$f_2(t) = \frac{m}{16\omega C}I_a\sin\left(2\omega t-\varphi\right). \tag{16}$$

When $m = 1, \varphi = 0, \omega = 314\,\mathrm{rad/s}$, the amplitude of the fundamental frequency is twice of the second harmonic from (15) and (16) as shown in Figs. 3(a) and 4(a).

2) Capacitor Voltage With Second Harmonic Eliminated: Similarly, capacitor voltage with eliminated second harmonic also means the elimination of the common part of the arm power. Let (11) be zero, the second harmonic component of the circulating current can be obtained as

$$i_{ha} = -\frac{m}{4}I_a\cos\left(2\omega t-\varphi\right) \tag{17}$$

Since the circulating current in MMC only contributes to the dc side, thus the component of the second harmonic in circulating current does influence the distribution of the dc source power and arm powers.

Substituting (17) into (12), we can obtain

$$p_{\mathrm{dif}} = \frac{2-m^2}{8}\cos\varphi V_{\mathrm{dc}}I_a\sin\omega t - \frac{2\sin\varphi}{4}V_{\mathrm{dc}}I_a\cos\omega t - \frac{m^2}{16}V_{\mathrm{dc}}I_a\sin(\omega t-\varphi)+\frac{m^2}{16}V_{\mathrm{dc}}I_a\sin(3\omega t-\varphi). \tag{18}$$

The differential-mode part of arm power in (18) only contains the fundamental and third harmonics. It can be concluded from (9) that the third harmonic in (18) results from the coupling between output voltage and second harmonic of circulating current.

Similarly, with (13) and (18), other harmonic components in SM capacitor voltage ripples can be obtained as

$$f_1(t) = -\frac{2-m^2}{8\omega C}\cos\varphi I_a\cos\omega t - \frac{2\sin\varphi}{4\omega C}I_a\sin\omega t + \frac{m^2}{16\omega C}I_a\cos(\omega t-\varphi) \tag{19}$$

$$f_3(t) = -\frac{m^2}{48\omega C}I_a\cos\left(3\omega t-\varphi\right). \tag{20}$$

It can be seen from (19) and (20) that amplitude of the fundamental frequency is three times than that of the third harmonic when $m = 1, \varphi = 0, \omega = 314\,\mathrm{rad/s}$ as shown in Figs. 3(b) and 4(b).

The above discussed two situations have shown different harmonics in capacitor voltage ripples by redistributing the powers among the arms.

It can be concluded that the general expression of the relationship between harmonics in SM capacitor voltage and arm powers can be expressed as

$$CV_{\mathrm{dc}}\sum_{i=1}^{\infty}\frac{df_i(t)}{dt} = \sum_{i=1}^{\infty}\frac{dp_i(t)}{dt} \tag{21}$$

where $p_i(t)$ is the *i*th harmonic component of the arm powers. Then, we can get the following expression:

$$f_i(t) = \frac{1}{i\omega C V_{\rm dc}} \int p_i(t) d(i\omega t). \tag{22}$$

Since the capacitor voltage and arm power are of the same frequencies, the high-frequency arm powers result in the high-frequency capacitor voltage ripples which are inversely proportional to its angular frequency in SM. So, it is significant for us to transfer the arm powers to the range of high frequency by redistributing the power to reduce the capacitor voltage ripples.

III. Hybrid MMC Topology With Redistributed Power

A. Analysis of SM Capacitor Voltage With Stored High-Frequency Power

For single SM as shown in Fig. 2, frequencies of the capacitor voltage are determined by the stored power of the single SM according to (4). Meanwhile, amplitude of the *i*th harmonic in SM capacitor voltage is inversely proportional to the *i*th angular frequency and SM capacitor value according to (22). Therefore, with rated reference voltage and current specified in the ac side and dc side, the reference power stored in SMs can be calculated. For the traditional MMC topology as shown in Fig. 2, the SM reference power is distributed in the range of the low frequencies, such as the fundamental frequency, the second-order harmonic, and third order harmonic, which would result in large SM capacitor voltage ripples for low-frequency output operation. It should be noted that frequency spectrum distribution in SM capacitor voltage is also related to the control strategy as discussed in Section II for the traditional MMC structure.

However, with inserted common-mode voltage and high-frequency circulating current presented in [15], the arm powers can be transferred into the high-frequency range which could reduce the capacitor voltage ripples dramatically. But, the reference voltage and current in the dc side and ac side are disturbed by the inserted voltage and current in [15]. Although the influence of the inserted current can be eliminated in feature of the three-phase MMC structure in dc side, ac-side reference voltage is disturbed with the inserted common-mode voltage. This issue inherently exists in the traditional MMC topology.

As the equivalent ac-side model discussed in the literature [21], the dynamic relation for the equivalent ac-side model can be expressed as

$$\sum_{i=1}^{n} \frac{1}{2}(u_{{\rm sm}(n+i)} - u_{{\rm sm}(n+1-i)}) - \frac{L}{2}\frac{di_a}{dt} = v_a. \tag{23}$$

Meanwhile, (23) can also be translated into the following equation:

$$\sum_{i=j+1}^{n} \frac{1}{2}\left(u_{{\rm sm}(n+i)} - u_{{\rm sm}(n+1-i)}\right) - \frac{L}{2}\frac{di_a}{dt} = v_a + \sum_{i=1}^{j} \frac{1}{2}\left(u_{{\rm sm}(n+1-i)} - u_{{\rm sm}(n+i)}\right). \tag{24}$$

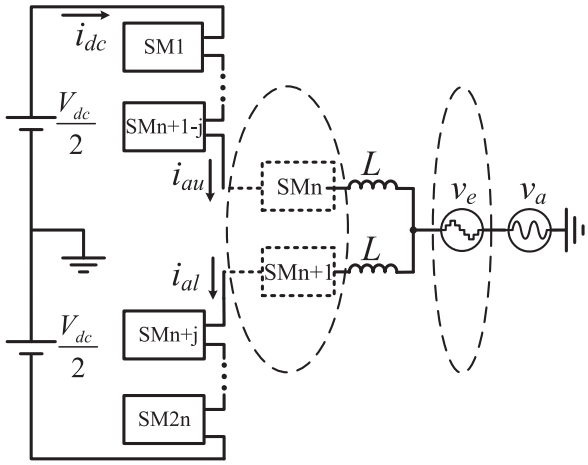

Fig. 5. Circuit of phase *a* of the hybrid MMC.

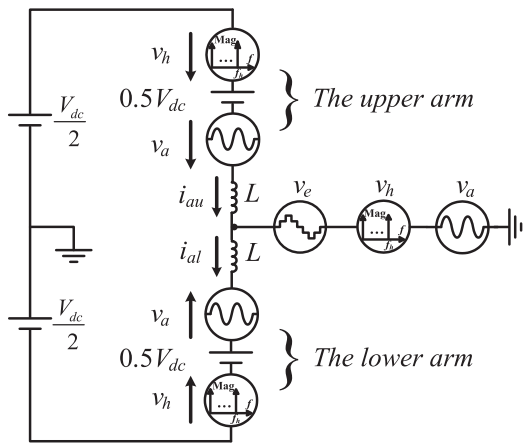

Fig. 6. Equivalent circuit of phase *a* based on (24).

As shown in Fig. 5, voltages of SMs in dashed line can be delivered to the ac side without changing the dynamic performance of the equivalent ac-side model according to (24). Fig. 6 shows the equivalent circuit structure of (24). The upper and lower arms both consist of the dc part, the fundamental part, and the high-frequency part. The variable voltage source v_e is the second term of the right-hand side of (24)

$$v_e = \sum_{i=1}^{j} \frac{1}{2}\left(u_{{\rm sm}(n+1-i)} - u_{{\rm sm}(n+i)}\right). \tag{25}$$

As shown in (25), the variable voltage source produced by the dashed SMs in Fig. 5 serves as an additional degree of freedom for providing the possibility of redistributing the arm powers by inserting the predominant high-frequency powers without disturbing the dc-side and ac-side references.

A suitable solution for power redistribution with hybrid MMC topology has been shown in Fig. 6. Three parts of SMs should be included in the proposed circuit. Two parts of those SMs are distributed in the upper and lower arms, and the third part is located in the ac side for producing the proposed variable voltage. In order to obtain the reduced capacitor voltage ripples in those SMs, it is necessary to handle the dominant

high-frequency powers in those SMs. Therefore, the independent high-frequency power source has to be performed to transfer the traditional low-frequency SM powers to the high-frequency range. Besides the inserted high-frequency voltages v_h in arms, which have opposite polarity without changing the equivalent dc-side model, the inserted high-frequency current i_h within the circulating current, which is independent of the inserted voltage, is also needed. Therefore, according to (9), arm powers of the proposed circuit can be obtained

$$\begin{cases} p'_{\rm up} = p_{\rm up} - v_h\left(i_{da} + \frac{1}{2}i_a\right) + \left(\frac{1}{2}V_{\rm dc} - v_a\right)i_h - v_h i_h \\ p'_{\rm low} = p_{\rm low} + v_h\left(i_{da} - \frac{1}{2}i_a\right) + \left(\frac{1}{2}V_{\rm dc} + v_a\right)i_h + v_h i_h \end{cases} \tag{26}$$

where $p'_{\rm up}$ and $p'_{\rm low}$ are upper arm power and lower arm power of the proposed circuit with high-frequency current and voltage inserted, respectively.

The common-mode power and the differential-mode power of the proposed circuit can also be expressed as

$$\begin{cases} p'_{\rm com} = \frac{1}{2}V_{\rm dc}i_{da} - \frac{1}{2}v_a i_a - \frac{1}{2}v_h i_a + \frac{1}{2}V_{\rm dc}i_h \\ p'_{\rm dif} = -v_a i_{da} + \frac{1}{4}V_{\rm dc}i_a - v_h i_{da} - v_a i_h - v_h i_h \end{cases}. \tag{27}$$

It can be seen from (27) that the first term and second term in right-hand side of the common-mode power contribute to the low-frequency power, and this can be eliminated by introducing the proper second-order harmonic into circulating current as discussed in Section II.

As for the differential-mode power in (27), the first two terms in right-hand side of the equation also serve as the low-frequency part. Different from the eliminated feature of the low-frequency power in common-mode power, the first two terms in right-hand side of differential-mode power cannot be eliminated mutually due to the limitation of the maximal value of the modulation index. Fortunately, these first two terms are both of the fundamental frequency, which can be eliminated or transferred into the high-frequency range by the independent differential-mode power $v_h i_h$. With computing resources and zero-crossing issue in the literature [15] taking into consideration, it is a wise choice to transfer the lower frequency power into the high-frequency area by properly controlling the independent power term $v_h i_h$.

With references specified in (5), the following equations can be obtained by substitution of (6)–(8) into (27)

$$\begin{cases} p'_{\rm com} = \frac{1}{2}V_{\rm dc}i_{ha} + \frac{m}{8}V_{\rm dc}I_a\cos 2\omega t - \frac{1}{2}v_h I_a \sin\omega t + \frac{1}{2}V_{\rm dc}i_h \\ p'_{\rm dif} = \frac{1}{8}(2-m^2)V_{\rm dc}I_a\sin\omega t - \frac{m}{4}v_h I_a - \frac{m}{2}V_{\rm dc}i_h - v_h i_h \end{cases}. \tag{28}$$

As we discussed above, low-frequency terms in arm powers cause the large fluctuations, and this influence can be suppressed according to the following equation:

$$\begin{cases} \frac{1}{2}V_{\rm dc}i_{da} - \frac{1}{2}v_a i_a = 0 \\ -v_a i_{da} + \frac{1}{4}V_{\rm dc}i_a - v_h i_h = p_h \end{cases} \tag{29}$$

where p_h expresses the equivalent high-frequency power stored in arms we preferred. Intention of the additional p_h is to avoid the zero-crossing computing issue of i_h. Therefore, the practicable scheme can be listed as

$$\begin{cases} i_{da} = -\frac{m}{4}I_a\cos\left(2\omega t - \varphi\right) \\ p_h = \frac{2-m^2}{8}V_{\rm dc}I_a\sin\omega t\,\cos 2\omega_h t \\ i_h = \frac{1}{V_h}\frac{2-m^2}{4}V_{\rm dc}I_a\sin\omega t\,\sin\omega_h t \\ v_h = V_h\sin\omega_h t \end{cases}. \tag{30}$$

It should be noted that frequency ω_h in v_h should be compromised between switching frequency and switching losses.

Since the inserted high-frequency circulating current i_h only flows around the dc side, the output power in Fig. 6 can be expressed as follows:

$$p_{\rm out} = v_e i_a + v_h i_a + v_a i_a. \tag{31}$$

The first term in the right-hand side of (31) is the power produced by the controllable voltage source, and the second term is the harmonics inserted in load power $v_a i_a$. In order to achieve the excellent load characteristic, the power effect of $v_h i_a$ should be eliminated by the controllable voltage source

$$v_e = -v_h. \tag{32}$$

As shown in (32), in order to obtain the precise high-frequency voltage, the cascaded FBSMs are hired to achieve the desirable v_e under control of the phase-shifted pulse width modulation (PWM) method as shown in Fig. 7. Fortunately, power $v_e i_a$ stored in the FBSMs locates in the range of high frequencies, which shows the much larger reduction in FBSM capacitor voltage ripples than the traditional topology.

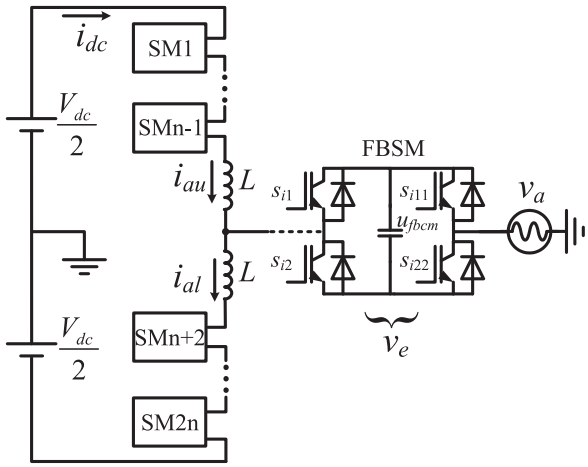

Fig. 7. Proposed hybrid MMC topology.

B. Analysis and Control of the Proposed FBSMs

The cascaded FBSMs of the hybrid MMC system are focusing on eliminating the common-mode voltage caused by the injected high-frequency voltage in the ac side. Meanwhile, power stored in the FBSMs is mainly the high-frequency harmonics. Therefore, the smaller rated power and larger reduction in FBSM capacitor voltage ripples can be achieved for each FBSM. Moreover, the small step voltages and low switching frequencies can also be achieved by the cascaded FBSM topology.

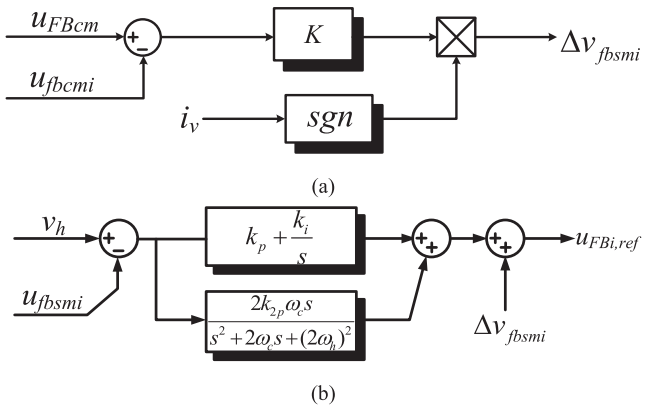

Fig. 8. Control structure of the proposed FBSMs. (a) Balancing control of the FBSMs. (b) PR control of output voltage of the FBSMs.

In the hybrid MMC system, all the FBSM capacitor voltage references are set to be equal to the arm SM capacitor voltage reference. In order to produce the excellent high-frequency voltage, sum of all the FBSM capacitor voltages should be at least equal to or larger than the amplitude of the high-frequency voltage. However, a compromise should be made between the cost and the performance. The maximum FBSM number is generally half of the SM number per arm.

The phase-shifted PWM method is hired for the cascaded FBSMs. For the hybrid MMC system with *j* FBSMs in the ac side, the reference modulation waveform of each FBSM is v_h/j, and the triangular carrier for each FBSM is shifted by $2\pi/j$ to achieve the harmonic cancellation.

Since the proposed cascaded FBSMs are located in the position of the ac side as shown in Fig. 7, the control strategy would be different from that in arms. Fig. 8 shows the control structure of the proposed FBSMs. The FBSM capacitor voltages should be balanced at its reference in order to produce the required controllable voltage v_e. As shown in Fig. 8, once the FBSM capacitor voltage deviates from its reference, the active power absorbed from load current would be produced to suppress its deviation. The voltage reference of the balancing control of the FBSMs can be represented as

$$\Delta v_{\mathrm{fbsm}i} = \begin{cases} K(u_{\mathrm{FBcm}} - u_{\mathrm{fbcm}i}), & i_v > 0 \\ -K(u_{\mathrm{FBcm}} - u_{\mathrm{fbcm}i}), & i_v < 0 \end{cases} \quad i = 1, 2, \ldots, j. \tag{33}$$

Fig. 9 shows the equivalent ac-side model of the proposed hybrid MMC topology. The reference voltage of the FBSM should be equal to the high-frequency voltage v_h. In order to obtain the stable ability in the ac side, the closed-loop regulator of the output voltage of FBSM should be applied. However, the PI controller is not available for tracking frequencies away from the dc part, especially for the high-frequency part. Therefore, a resonant controller with the resonant angle frequency ω_h is adopted for the FBSMs as shown in Fig. 8(b).

Note that balance of each FBSM is based on the balance of power stored in each FBSM in a specified period. The active

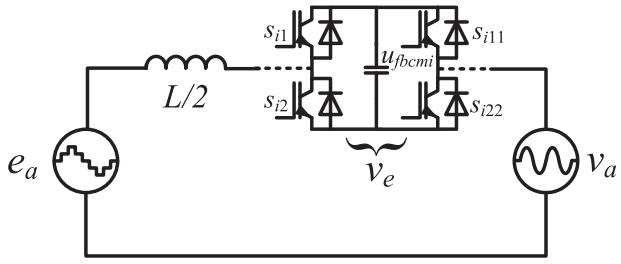

Fig. 9. Equivalent ac-side circuit model of the proposed MMC topology.

power stored in each FBSM during a fundamental period can be expressed as

$$p_{\mathrm{FB}i} = \frac{\omega}{2\pi} \int_{t_0}^{t_0 + 2\pi/\omega} u_{\mathrm{fbsm}i} \cdot i_v dt \tag{34}$$

where $p_{\mathrm{FB}i}$ is the active power of the *i*th FBSM, $u_{\mathrm{fbsm}i}$ is the output voltage of the *i*th FBSM, and t_0 is the initial time of the integral. According to the control strategy, the aim of the FBSMs is to eliminate the high-frequency part v_h in the ac side based on (32). Therefore, frequencies of the FBSM output voltages are distributed in both the frequency of inserted high-frequency v_h and the higher frequencies produced by the PWM modulation process. So, the FBSM output voltages show the different frequencies with the fundamental frequency in the load current. It is assumed that the switching losses are ignored in (34). Based on the orthogonal theorem of the trigonometric function, we can obtain

$$p_{\mathrm{FB}i} = 0. \tag{35}$$

Equation (35) shows that the capacitor voltages in the FBSMs would keep balanced in fundamental period with the balancing control. And the FBSMs would not influence the active power distribution of the proposed hybrid MMC system. Therefore, the FBSMs function as the harmonic power generator redistributing the harmonics among the MMC system. This is different from SMs in arms which only contain the active power and reactive power.

C. Maximum Output Voltage of the Proposed Topology

According to the literature [22], range of the equivalent inner electromotive force (EMF) shown in Fig. 9 of the proposed MMC topology can be expressed as

$$\max\left\{-\frac{V_{\mathrm{dc}}}{2}, \frac{V_{\mathrm{dc}}}{2} - (n-j)u_{\mathrm{cm}}\right\} \leq e_x \leq \min\left\{\frac{V_{\mathrm{dc}}}{2}, (n-j)u_{\mathrm{cm}} - \frac{V_{\mathrm{dc}}}{2}\right\}. \tag{36}$$

In order to obtain the maximum symmetrical ac voltage of the arms, the SM reference voltage in arm can be designed as

$$u_{\mathrm{cm}} = \frac{V_{\mathrm{dc}}}{n-j}. \tag{37}$$

Similarly, range of the output voltage of the FBSMs can be expressed as

$$-ju_{\mathrm{fbcm}} \leq u_{\mathrm{fbsm}} \leq ju_{\mathrm{fbcm}}. \tag{38}$$

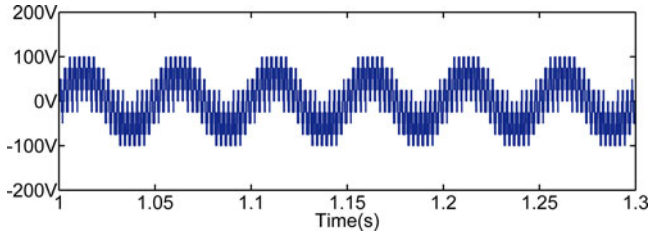

Fig. 10. Waveform of e_v for the proposed MMC topology.

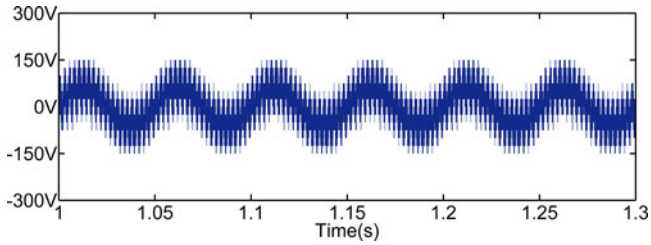

Fig. 11. Waveform of $e_x + u_{\mathrm{fbsm}}$ for the proposed MMC topology with one FBSM in the ac side.

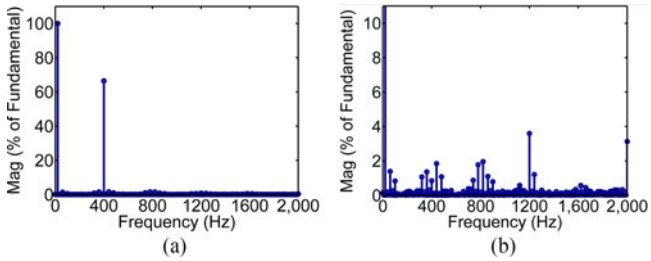

Fig. 12. Voltage frequency distribution when $m = 0.6$, $\varphi = 0$, $\omega = 125.6$ rad/s, $j = 1$. (a) Voltage frequency distribution of e_x. (b) Voltage frequency distribution of $e_x + u_{\mathrm{fbsm}}$.

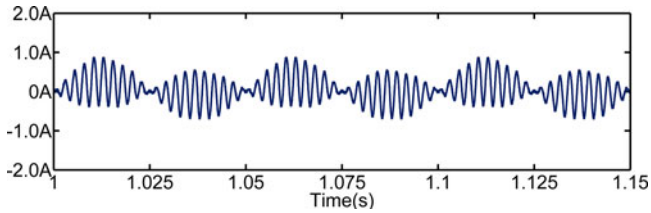

Fig. 13. Upper arm current of the proposed MMC topology.

Due to the modularity feature in MMC, it is significant to make all the capacitor values identical. Therefore, based on (36)–(38), range of the output voltage of the proposed hybrid MMC can be expressed as

$$-\frac{V_{\mathrm{dc}}}{2}\frac{n+j}{n-j} \le e_x + u_{\mathrm{fbsm}} \le \frac{V_{\mathrm{dc}}}{2}\frac{n+j}{n-j}. \tag{39}$$

It can be seen from (39) that the modulation index of the proposed MMC topology can be enlarged compared with the traditional MMC topology. Fig. 10 shows the EMF waveform e_x of the hybrid MMC topology with one FBSM inserted in the ac side. Fig. 11 shows the waveform of $e_x + u_{\mathrm{fbsm}}$ with the enlarged output voltage which is in accord with (39).

Moreover, it can be seen from Fig. 12 that the inserted v_h in e_x shown in Fig. 10 has almost been eliminated in $e_x + u_{\mathrm{fbsm}}$ shown in Fig. 11. Harmonics of $e_x + u_{\mathrm{fbsm}}$ occupy the range of high frequencies with relatively small content, which can be easily filtered by the equivalent inductor as shown in Fig. 9.

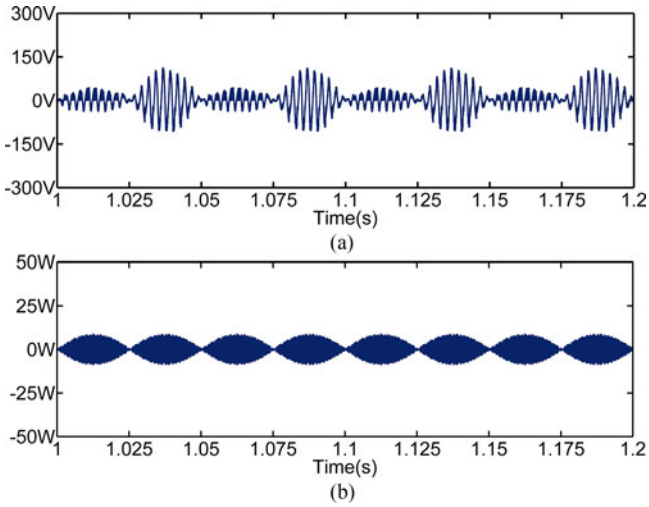

Fig. 14. Power in SM and FBSM with $m = 0.6, \varphi = 0, \omega = 125.6$ rad/s. (a) Power in SM. (b) Power in FBSM.

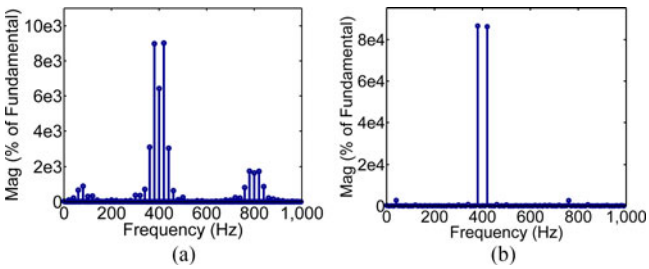

Fig. 15. Power frequency distribution with $m = 0.6, \varphi = 0, \omega = 125.6$ rad/s. (a) Arm power frequency distribution. (b) FBSM power frequency distribution.

TABLE I
CIRCUIT PARAMETERS FOR SIMULATION

Symbol	Quantity	Value
V_{dc}	DC-link voltage	200 V
N	Number of SMs per arm	4
j	Number of FBSMs per phase	2
ω	Line angle frequency	125.6 rad/s
C	SM capacitor value	1 mF
C_f	FBSM capacitor value	1 mF
L	Arm inductor	10 mH
f_c	SM switching frequency	1 kHz
f_{fc}	FBSM switching frequency	1 kHz
f_{com}	Frequency of inserted common voltage	400 Hz
u_{cm}	SM capacitor voltage reference	50 V
u_{FBcm}	FBSM capacitor voltage reference	50 V
m	SM modulation index	0.6
m_f	FBSM modulation index	0.4
R_{load}	Load resistance	180 Ω

IV. SIMULATION RESULT

With the detailed discussion of the hybrid MMC topology mentioned above, the MATLAB/Simulink is hired to achieve the verification. Basic circuit topology is based on Fig. 7. The phase-shifted carrier PWM (PSC-PWM) is adopted for both

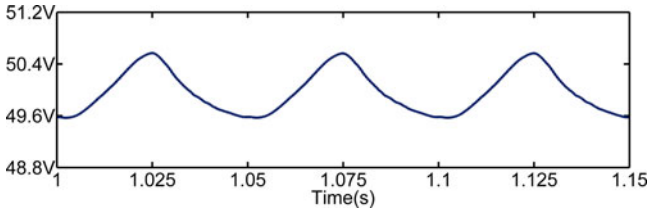

Fig. 16. SM capacitor voltage of the traditional MMC topology.

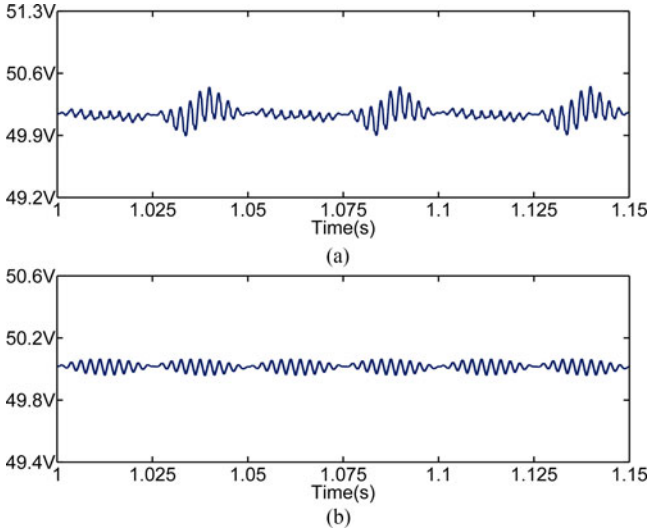

Fig. 17. SM capacitor voltage with $m = 0.6, \varphi = 0, \omega = 125.6$ rad/s. (a) SM capacitor voltage in arms. (b) FBSM capacitor voltage.

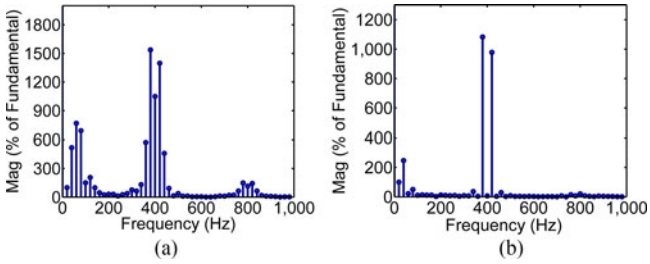

Fig. 18. SM capacitor voltage frequency distribution with $m = 0.6$, $\varphi = 0$, $\omega = 125.6$ rad/s. (a) SM capacitor voltage frequency distribution for arms. (b) FBSM capacitor voltage frequency distribution.

the arm SMs and the FBSM. Detailed simulation parameters are listed in Table I.

Fig. 13 shows the upper arm current of the hybrid MMC. Fig. 16 shows the SM capacitor voltage of the traditional MMC topology with the low-frequency feature and the large ripple. Fig. 17 shows the simulated capacitor voltage of both the arm SM and the FBSM under the proposed MMC topology. It can be seen that the capacitor voltage ripple in arm SM of the hybrid topology is less than half of the capacitor voltage ripple of the traditional topology as shown in Figs. 16 and 17(a). Fig. 17(b) shows that the capacitor voltage ripple in FBSM is much smaller than that in arm SM. And it is reasonable for what we discussed based on Figs. 18 and 22. The voltage frequency distribution of arm SM and FBSM shown in Fig. 18 has the similar frequency distribution with the stored powers in arm SMs and FBSM with

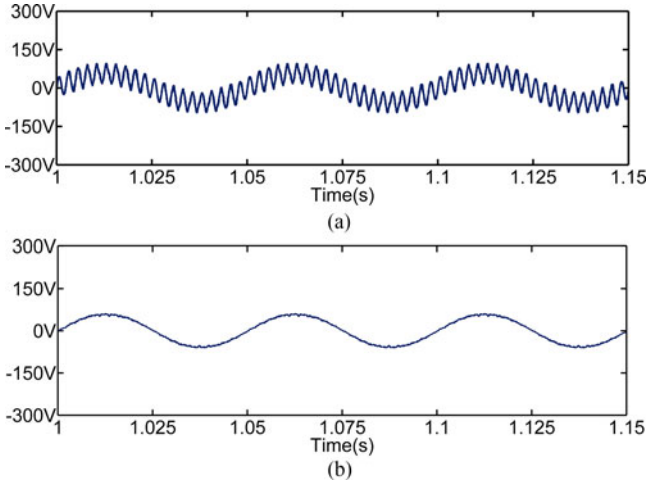

Fig. 19. Output voltage frequency distribution with $m = 0.6$, $\varphi = 0$, $\omega = 125.6$ rad/s. (a) Output voltage without FBSMs. (b) Output voltage with FBSMs.

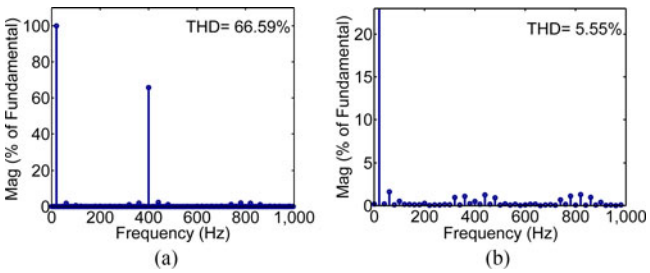

Fig. 20. Output voltage frequency distribution with $m = 0.6$, $\varphi = 0$, $\omega = 125.6$ rad/s. (a) Output voltage without FBSM. (b) Output voltage with FBSM.

that in Fig. 15. This is because each harmonic in SM capacitor voltage is proportional to its corresponding harmonic of the stored power in SM approximately. Due to the assumption that the ripples in capacitor voltage are negligible compared with the SM reference capacitor voltage based on (4), it shows that frequency distribution of the powers and capacitor voltages shown in Figs. 14 and 17 still has a little difference with that in Figs. 15 and 18. In other words, with the increasing proportion of the capacitor voltage ripple to the capacitor voltage reference, there will be aggravating difference as shown in Figs. 15 and 18.

The main point of the proposed hybrid MMC topology is to reduce the SM capacitor voltage ripples, as well as keep the output voltage free of the inserted common-mode voltage v_h. Fig. 19 shows the output voltages of the traditional MMC and hybrid MMC with high-frequency powers inserted in arms. Fig. 20 shows the frequency spectrum of Fig. 19. The output voltage with common-mode voltage v_h inserted based on the traditional MMC topology is shown in Fig. 19(a). Fig. 20(a) shows its frequency spectrum, it can be seen that the output voltage of the traditional MMC topology consists of the fundamental frequency part and the undesirable high-frequency part. With the FBSM acting as the harmonic power generator to eliminate the harmonic power in the ac side, the output voltage has shown noticeable improvement as shown in Figs. 19 and 20. The total harmonic distortion (THD) of the output voltage has

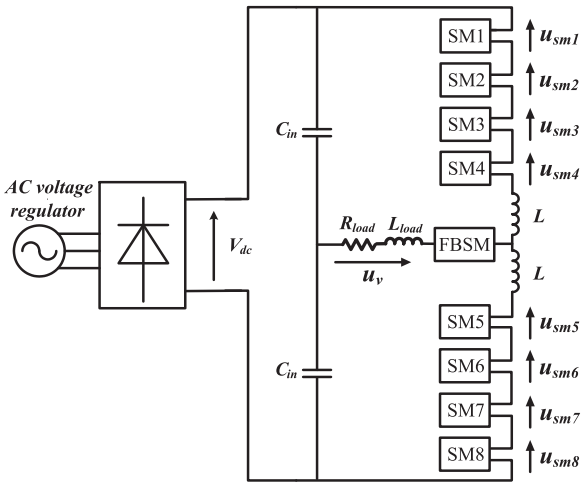

Fig. 21. Experimental circuit of the proposed MMC system.

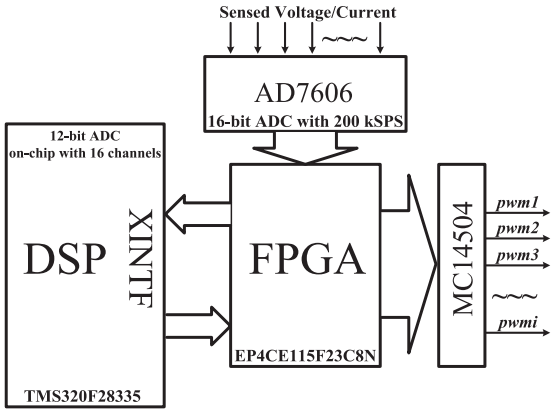

Fig. 22. Detailed structure of the control system.

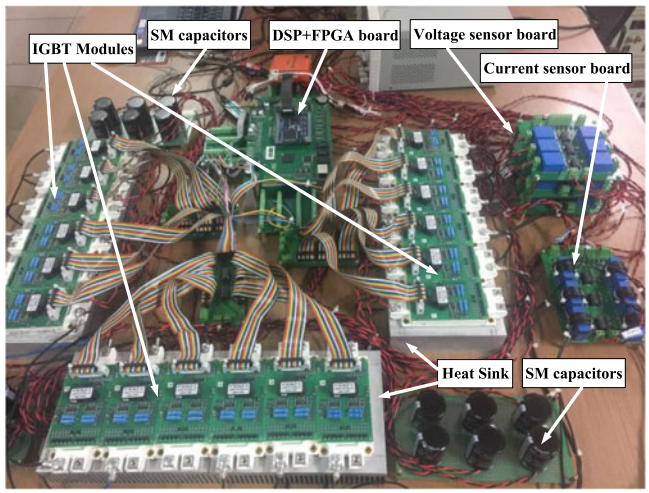

Fig. 23. Experimental photograph of the proposed hybrid MMC system.

TABLE II
CIRCUIT PARAMETERS FOR EXPERIMENT

Symbol	Quantity	Value
$C_{\rm in}$	Input electrolytic capacitor	10 mF
$V_{\rm dc}$	DC-link voltage	200 V
N	Number of SMs per arm	4
j	Number of FBSMs per phase	2
ω	Line angle frequency	125.6 rad/s
C	SM capacitor value	1 mF
C_f	FBSM capacitor value	1 mF
L	Arm inductor	6 mH
f_c	SM switching frequency	1 kHz
f_{fc}	FBSM switching frequency	1 kHz
$f_{\rm com}$	Frequency of inserted common voltage	400 Hz
$f_{\rm samp}$	Sample rate	10 kHz
$u_{\rm cm}$	SM capacitor voltage reference	50 V
$u_{\rm fbcm}$	FBSM capacitor voltage reference	50 V
m	SM modulation index	0.6
m_f	FBSM modulation index	0.4
$R_{\rm load}$	Load resistance	50 Ω

been reduced dramatically from 66.59% to 5.55% with the proposed topology. It should be noted that proposed FBSM with the PSC-PWM method would introduce harmonics related to its switching frequency in the ac side. However, these harmonics can be suppressed by the arm inductors since the inductors take effect in the ac side based on (24).

V. EXPERIMENTAL RESULT

For the better verification of the hybrid MMC topology research, a prototype of the hybrid MMC system with eight SMs per phase has been developed as shown in Fig. 21. This prototype consists of the power stage and the control board. The power stage working under the inverter mode has eight half-bridge based SMs and one full-bridge based SM. A three-phase uncontrolled rectifier with electrolytic capacitors constitutes the dc bus voltage. For driving large numbers of the SMs, the TMS32 0f 28335 DSP chip which only contains 12 PWM signals is no longer suitable. Therefore, an EP4CE115F23C8N field-programmable gate array (FPGA) chip is hired for its large numbers of IOs and the powerful parallel algorithm. Detailed control structure is shown in Fig. 22. The DSP chip acting as the host chip achieves the control algorithm and communicates with the synergy FPGA chip for obtaining the sensed signals. The FPGA chip receives the modulation waveform from the DSP chip and achieves the PWM modulation process. The final PWM signals are also produced by the FPGA chip. Experimental photograph of the hybrid MMC system is shown in Fig. 23. Detailed experimental parameters are listed in Table II.

Fig. 24 shows the upper arm and the lower arm currents of the hybrid MMC topology. It can be seen that the arm currents have fluctuation relevant to the inserted high-frequency current.

The traditional MMC system without the proposed ac-side FBSM is also experimented. Fig. 25 shows the SM capacitor voltage. It shows that the peak-to-peak ripple of the traditional SM capacitor voltage is almost 6 V, which is relatively high with the 12% ripple compared with the reference voltage 50 V. The SM capacitor voltage of the hybrid MMC topology is shown in Fig. 26. It can be seen that the peak-to-peak ripple (almost 3 V) has been dramatically reduced compared with the capacitor voltage ripple in Fig. 25. It shows that the capacitor voltage in Fig. 26 fluctuates more frequently than that of the voltage in Fig. 25.

The output voltage, arm current, and inserted power in SM1 have also been shown in Fig. 27. The SM power shown in Fig. 27

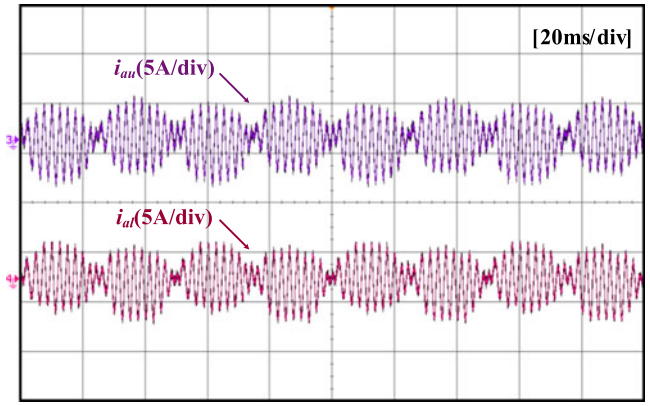

Fig. 24. Experimental results of upper and lower arm currents of the hybrid MMC topology.

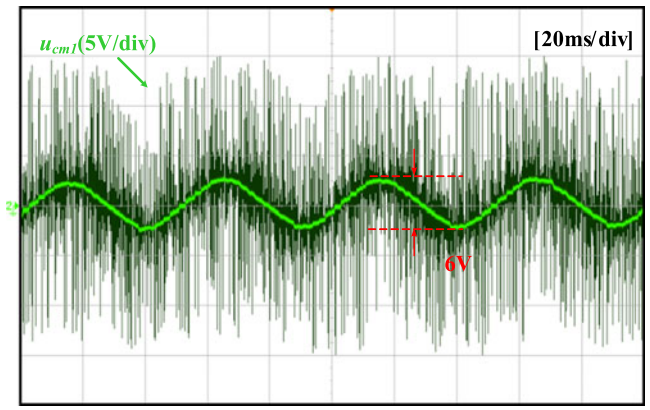

Fig. 25. Experimental result of SM capacitor voltage of the traditional MMC topology.

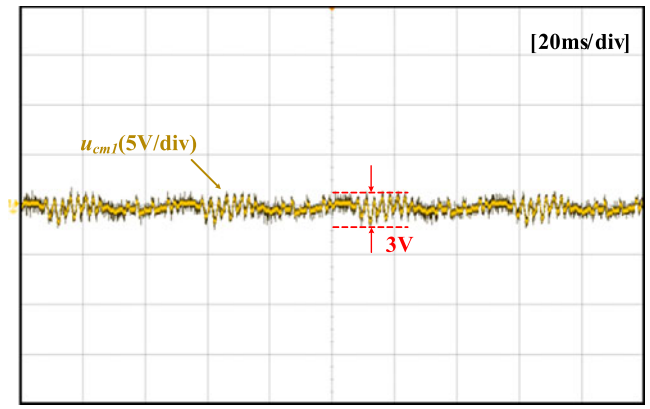

Fig. 26. Experimental result of SM capacitor voltage of the hybrid MMC topology.

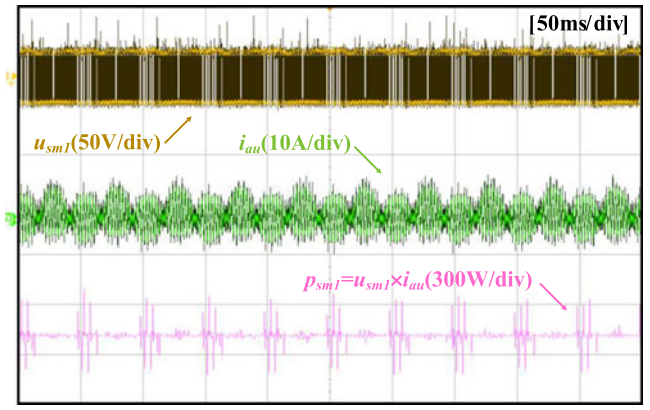

Fig. 27. Experimental result of SM output voltage, arm current, and power inserted in SM1 of the hybrid MMC topology.

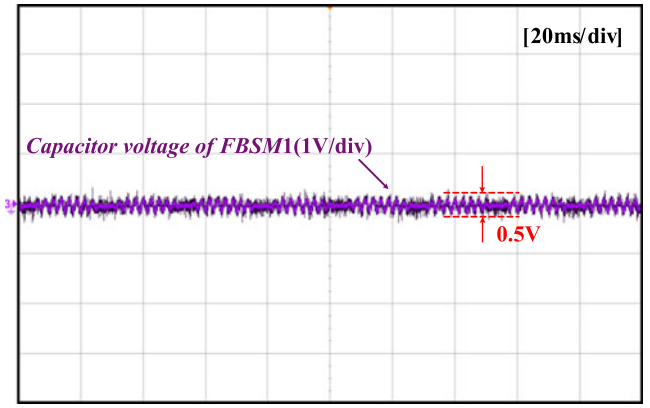

Fig. 28. Experimental result of FBSM capacitor voltage of the hybrid MMC topology.

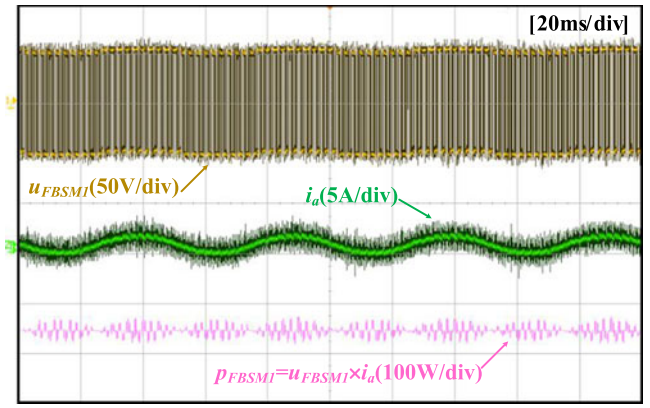

Fig. 29. Experimental result of the FBSM output voltage, load current, and power inserted in FBSM of the hybrid MMC topology.

has the similar feature with that in Fig. 14(a). Fig. 28 shows the inserted FBSM capacitor voltage. Different with powers frequencies including both the low-frequency components and high-frequency components of the arm SMs, the stored power in FBSM only has the high-frequency components, which means the lower ripple obtained by the FBSM. As shown in Fig. 28, the FBSM capacitor voltage ripple is 0.5 V. The corresponding FBSM output voltage, load current, and stored power in FBSM are shown in Fig. 29. It is obvious that power fluctuation in FBSM shows larger reduction than that inserted in arm SMs as shown in Fig. 27.

With the above-mentioned experimental results discussed, the arm SMs and FBSM capacitor voltage ripples of the hybrid MMC system have been reduced dramatically by redistributing the arm powers in SMs. Moreover, the ac-side power is redistributed with help of the proposed harmonic power generator FBSM. Fig. 30 shows the output voltage with the inserted

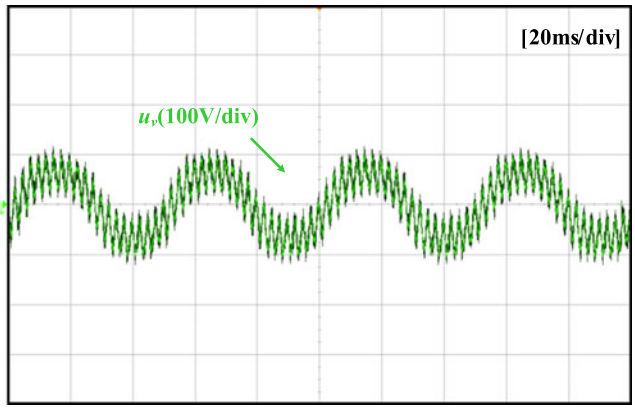

Fig. 30. Experimental result of the output voltage without the proposed FBSM.

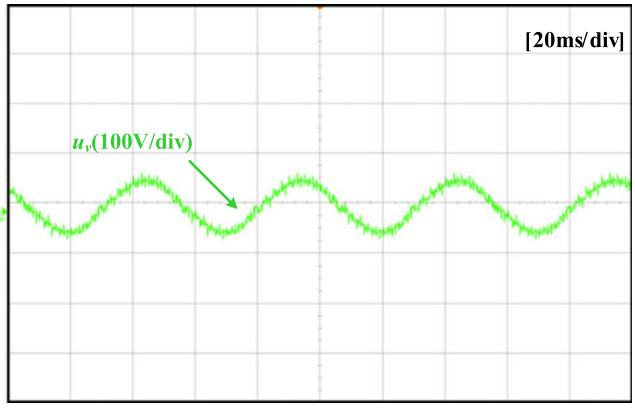

Fig. 31. Experimental result of the output voltage of the hybrid MMC topology.

common-mode voltage without the proposed FBSM in the ac side. The output voltage in Fig. 30 is distorted by the inserted common-mode voltage without the proposed FBSM. The output voltage of the hybrid MMC topology is shown in Fig. 31. It shows that the output voltage in Fig. 31 has been improved dramatically. The common-mode voltage in Fig. 30 has been eliminated by the proposed FBSMs.

VI. Conclusion

This paper has introduced a hybrid MMC topology with inserted FBSMs in the ac side for redistributing the powers among the SMs and the proposed FBSMs, which aims to reduce the capacitor voltage ripples of the SMs and FBSMs without disturbing the output voltage in the ac side. As the above-mentioned analysis we discussed, the SM capacitor voltage ripples can be dramatically reduced by transferring the frequency spectrum of SM powers into the range of the high-frequency area with the hybrid MMC topology. Actually, the proposed FBSMs function as the harmonic power generator in the hybrid MMC topology for eliminating the ac-side harmonic power produced by the inserted common-mode voltage. Moreover, modulation index can be enlarged by the hybrid MMC. Simulation and experimental results have verified the excellent performance of the hybrid MMC.

References

[1] A. Lesnicar and R. Marquardt, "An innovative modular multilevel converter topology suitable for a wide power range," in *Proc. IEEE Power Tech Conf.*, Jun. 2003, pp. 1–6.
[2] M. Glinka and R. Marquardt, "A new ac/ac multilevel converter family," *IEEE Trans. Ind. Electron.*, vol. 52, no. 3, pp. 662–669, Jun. 2005.
[3] M. Glinka, "Prototype of multiphase modular-multilevel converter with 2 MW power rating and 17-level-output-voltage," in *Proc. IEEE Power Electron. Spec. Conf.*, 2004, pp. 2572–2576.
[4] S. Allebrod, R. Hamerski, and R. Marquardt, "New transformerless, scalable modular multilevel converters for HVDC-transmission," in *Proc. IEEE Trans. Power Electron. Spec. Conf.*, Jun. 2008, pp. 174–179.
[5] H. Akagi, "Classification, terminology, and application of the modular multilevel cascade converter (MMCC)," *IEEE Trans. Power Electron.*, vol. 26, no. 11, pp. 3119–3130, Nov. 2011.
[6] J. Rodriguez, S. Bernet, P. K. Steimer, and I. E. Lizama, "A survey on neutral-point-clamped inverters," *IEEE Trans. Ind. Electron.*, vol. 57, no. 7, pp. 2219–2230, Jul. 2010.
[7] Z. Li, P. Wang, Z. Chu, H. Zhu, Y. Luo, and Y. Li, "An inner current suppressing method for modular multilevel converters," *IEEE Trans. Power Electron.*, vol. 28, no. 11, pp. 4873–4879, Nov. 2013.
[8] M. Zhang, L. Huang, W. Yao, and Z. Lu, "Circulating harmonic current elimination of a CPS-PWM-Based modular multilevel converter with a plug-in repetitive controller," *IEEE Trans. Power Electron.*, vol. 29, no. 4, pp. 2083–2097, Apr. 2014.
[9] F. Deng and Z. Chen, "Voltage-balancing method for modular multilevel converters switched at grid frequency," *IEEE Trans. Ind. Electron.*, vol. 62, no. 5, pp. 2835–2847, May 2015.
[10] F. Deng and Z. Chen, "Voltage-balancing method for modular multilevel converters under phase-shifted carrier-based pulsewidth modulation," *IEEE Trans. Ind. Electron.*, vol. 62, no. 7, pp. 4158–4169, Jul. 2015.
[11] B. Li, Y. Zhang, G. Wang, W. Sun, D. Xu, and W. Wang, "A modified modular multilevel converter with reduced capacitor voltage fluctuation," *IEEE Trans. Power Electron.*, vol. 62, no. 10, pp. 6108–6119, Oct. 2015.
[12] M. Hagiwara, K. Nishimura, and H. Akagi, "A medium-voltage motor drive with a modular multilevel converter PWM inverter," *IEEE Trans. Power Electron.*, vol. 25, no. 7, pp. 1786–1799, Jul. 2010.
[13] A. Antonopoulos, L. Angquist, S. Norrga, K. Ilves, L. Harnefors, and H.-P. Nee, "Modular multilevel converter ac motor drives with constant torque from zero to nominal speed," *IEEE Trans. Ind. Appl.*, vol. 50, no. 3, pp. 1982–1993, May/Jun. 2014.
[14] S. Debnath, J. Qin, and M. Saeedifard, "Control and stability analysis of modular multilevel converter under low-frequency operation," *IEEE Trans. Ind. Electron.*, vol. 62, no. 9, pp. 5329–5339, Sep. 2015.
[15] A. J. Korn, M. Winkelnkemper, and P. Steimer, "Low output frequency operation of the modular multi-level converter," in *Proc. IEEE Energy Convers. Congr. Expo. Conf.*, Sep. 2010, pp. 3993–3997.
[16] M. Hagiwara, I. Hasegawa, and H. Akagi, "Start-Up and low-speed operation of an electric motor driven by a modular multilevel cascade inverter," *IEEE Trans. Ind. Appl.*, vol. 49, no. 4, pp. 1556–1565, Jul./Aug. 2013.
[17] K. Wang, Y. Li, Z. Zheng, and L. Xu, "Voltage balancing and fluctuation-suppression methods of floating capacitors in a new modular multilevel converter," *IEEE Trans. Ind. Electron.*, vol. 60, no. 5, pp. 1943–1954, May 2013.
[18] S. Du, B. Wu, N. R. Zargari, and Z. Cheng, "A flying-capacitor modular multilevel converter for medium-voltage motor drive," *IEEE Trans. Power Electron.*, vol. 32, no. 3, pp. 2081–2089, Mar. 2017.
[19] R. Li, G. P. Adam, D. Holliday, J. E. Fletcher, and B. W. Williams, "Hybrid cascaded modular multilevel converter with dc fault ride-through capability for the HVDC transmission system," *IEEE Trans. Power Del.*, vol. 30, no. 4, pp. 1853–1862, Aug. 2015.
[20] M. Hagiwara and H. Akagi, "Control and experiment of pulsewidth-modulated modular multilevel converters," *IEEE Trans. Power Electron.*, vol. 24, no. 7, pp. 1737–1746, Jul. 2009.
[21] M. Huang, J. Zou, and X. Ma, "An improved phase-shifted carrier modulation for modular multilevel converter to suppress the influence of fluctuation of capacitor voltage," *IEEE Trans. Power Electron.*, vol. 31, no. 10, pp. 7404–7416, Oct. 2016.
[22] L. He, K. Zhang, J. Xiong, S. Fan, and Y. Xue, "Low-frequency ripple suppression for medium-voltage drives using modular multilevel converter with full-bridge submodules," *IEEE J. Emerging Sel. Topics Power Electron.*, vol. 4, no. 2, pp. 657–667, Jun. 2016.

Ming Huang was born in 1989. He received the B.S. degree in electrical engineering in 2011 from Hefei University of Technology, Hefei, China. He is currently working toward the Ph.D. degree at Xi'an Jiaotong University, Xi'an, China.

His current research interest focuses on modular multilevel converters in medium-high power applications.

Jianlong Zou was born in Shandong, China, in 1976. He received the B.Sc., M.Sc., and Ph.D. degrees in electrical engineering from Xi'an Jiaotong University, Xi'an, China, in 1999, 2002, and 2008, respectively.

In 2002, he joined the Faculty of Electrical Engineering, Xi'an Jiaotong University, where he is currently an Associate Professor. He has good cooperation with The Hong Kong Polytechnic University. In 2012, he was a Visiting Scholar with Michigan State University. His main areas of research interests include modular multilevel converter based HVDC, wind generation, and nonlinear dynamics in electrical engineering.

Xikui Ma was born in Shaanxi, China, in 1958. He received the B.Sc. and M.Sc. degrees in electrical engineering from Xi'an Jiaotong University, Xi'an, China, in 1982 and 1985, respectively.

In 1985, he joined as a Lecturer in the Faculty of Electrical Engineering, Xi'an Jiaotong University, where he became a Professor in 1992. During the academic year 1994–1995, he was a Visiting Scientist in the Department of Electrical Engineering and Computer, University of Toronto. He is the Author or Coauthor of more than 140 scientific and technical papers on these subjects, and also the author of five books in electromagnetic fields. His current research interests include electromagnetic field theory and its applications, analytical and numerical methods in solving electromagnetic problems, chaotic dynamics and its applications in power electronics, and the applications of digital control to power electronics.